Whole cell based electrical impedance sensing approach for a rapid nanotoxicity assay

2010 Nanotechnology 21 315103

(http://iopscience.iop.org/0957-4484/21/31/315103)

Nanotechnology **21** (2010) 315103 (9pp) doi:10.1088/0957-4484/21/31/315103

Whole cell based electrical impedance sensing approach for a rapid nanotoxicity assay

Evangelia Hondroulis, Chang Liu and Chen-Zhong Li[1]

Nanobioengineering/Bioelectronics Laboratory, Department of Biomedical Engineering, Florida International University, 10555 West Flagler Street, Miami, FL 33174, USA

E-mail: licz@fiu.edu

Received 18 February 2010, in final form 16 June 2010
Published 12 July 2010
Online at stacks.iop.org/Nano/21/315103

Abstract

A whole cell based biosensor for rapid real-time testing of human and environmental toxicity of nanoscale materials is reported. Recent studies measuring nanoparticle cytotoxicity *in vitro* provide a final measurement of toxicity to a cell culture overlooking the ongoing cytotoxic effects of the nanoparticles over the desired timeframe. An array biosensor capable of performing multiple cytotoxicity assays simultaneously was designed to address the need for a consistent method to measure real-time assessments of toxicity. The impedimetric response of human lung fibroblasts (CCL-153) and rainbow trout gill epithelial cells (RTgill-W1) when exposed to gold and silver nanoparticles (AuNPs, AgNPs), single walled carbon nanotubes (SWCNTs) and cadmium oxide (CdO) was tested. Exposure to CdO particles exhibited the fastest rate of cytotoxicity and demonstrated the biosensor's ability to monitor toxicity instantaneously in real time. Advantages of the present method include shorter run times, easier usage, and multi-sample analysis leading to a method that can monitor the kinetic effects of nanoparticle toxicity continuously over a desired timeframe.

(Some figures in this article are in colour only in the electronic version)

1. Introduction

Nanotechnology has great potential benefits in rapidly developing fields such as biomedical engineering, drug delivery, environmental health, pharmaceutical industries and even electronics and communication technologies. For instance, in the healthcare field, nanomaterials are being considered in the development of new drugs and new therapies for disease control and improving the quality of life. More recently, nanomaterials have been used in tissue engineering and medical imaging, leading to improved diagnostics and new therapeutic treatments. However, with this rapid development, these new nanoscale materials (including nanotubes, nanowires, nanowhiskers, fullerenes or buckyballs and quantum dots) might have unintended hazards for human health and the environment (Oberdörster *et al* 2005, Kreyling *et al* 2006).

Testing for toxicological parameters is a necessary first step toward ensuring the compatibility of nanomaterials for medical applications and for the safety of the environment. The properties of metals change when they are in the nanoscale and they may pose certain threats to biological systems that their bulk counterparts may not. To date, nanotoxicity is a crucial topic that is being addressed by a number of studies (Soto *et al* 2005); however, there is a lack of consensus in the published literature on nanoparticle toxicity due to the variability of methods, materials and cell lines used (Lewinski *et al* 2008). With the increase in research and commercial use of these nanomaterials, standardization of methods in nanotoxicity testing is becoming increasingly important to validate these novel techniques.

The main risk associated with the use and manufacture of nanomaterials is human and environmental exposure. One of the more common impacts of the use of nanomaterials is the emission of hazardous air pollutants which contain particulate matter on the order of 1–100 nm in size. Any material in the

[1] Author to whom any correspondence should be addressed.

respirable size range, less than 100 nm in diameter, may have toxic effects on the lung fibroblasts after inhalation (Mossman *et al* 2007). In particular, nanoparticles with sizes less than 20 nm affect the alveolar region of the lung, and therefore human lung fibroblasts (CCL-153) were chosen for this study (Elder *et al* 2009). More recently, the use of nanomaterials in biomedical sciences has placed nanomaterials directly in contact with biological materials, and thus it is necessary to observe their interaction closely.

In the environment, nanotechnology is being used to solve problems such as soil and groundwater remediation, air purification, pollution detection and sensing. Manufactured nanoparticles are being engineered for projects that will benefit the environment as well in the form of environmental clean-up tools, for example for groundwater for remediation. For instance, in the UN Millennium Project, fullerenes are being used to absorb various toxins and iron nanoparticles to catalyze the breakdown of solvents. There have been debates on whether the disposal of these manufactured nanoparticles causes significant harm to the environment as there is a lack of validated protocols for their disposal and removal (Ghosh *et al* 2008). For this matter, rainbow trout gill epithelial cells (RTgill-W1) were also tested as the destination of the nanoparticles after disposal may be groundwater and eventually aquatic systems.

Traditional biological methods for measurement of cellular activity and proliferation are used in current nanotoxicity studies. These methods include mitochondrial reduction of tetrazolium salts into an insoluble dye (the MTT test) and enzyme lactate dehydrogenase (LDH) release tests. These methods are used as markers for cell viability and consist of procedures that provide a general sense of cytotoxicity as they show results only at a final time point (Hussain *et al* 2005). As a result, the kinetic model (absorption, distribution, metabolism and excretion) of the nanoparticle uptake is not usually observed with these conventional methods. Following biological exposure, the particles may transport across cell membranes, especially into mitochondria, causing internal damage that may affect cell behavior and over time, lead to cell death (Wilhelm *et al* 2002).

Biosensors are becoming valuable tools for detecting toxic chemical compounds in industrial products, chemical substances, environmental samples (e.g. air, soil and water) or biological systems (e.g. bacteria, viruses or tissue components). Most current biosensors are used to detect enzymes, DNA/RNA and immunological components (Luong *et al* 2008). Biosensors that incorporate whole cells can have an advantage over these previous biosensors as they are able to provide information about the total physiological effect of a toxin towards the whole cell. In this study, we designed an array-formatted whole cell based electrical impedance sensing system (EIS) that is capable of revealing the kinetic effects of gold nanoparticles (AuNPs; 10, 100 nm), silver nanoparticles (AgNPs; 10, 100 nm), single walled carbon nanotubes (SWCNTs; cut, uncut) and cadmium oxide (CdO) when in contact with CCL-153 and RTgill-W1 cells. The EIS measures the resistance produced by growing cell monolayers over electrodes and can detect changes in resistance that may occur with changes in the cell layer after nanoparticle exposure. The EIS offers compact structure, ease of use and the ability to measure multiple samples simultaneously in real time, a critical feature in monitoring cytotoxicity. The results obtained from the EIS studies were compared to the Sulforhodamine B colorimetric (SRB) assay commonly used for cytotoxicity screening.

2. Experimental details

2.1. Chemicals and reagents

Acetone, isopropyl alcohol (IPA), phosphate-buffered saline (PBS), sodium phosphate (Na_2HPO_4), potassium dihydrogen phosphate (KH_2PO_4), potassium chloride (KCl), sodium hydroxide (NaOH), hydrogen tetrachloroaurate ($HAuCL_4$), trisodium citrate ($Na_3C_6H_5O_7$), sodium borohydride ($NaBH_4$), silver nitrate ($AgNO_3$), sulfuric acid (H_2SO_4) nitric acid (HNO_3), trichloroacetic acid and acetic acid were all purchased from Fisher. CdO and SWCNTs were purchased from Sigma Aldrich.

2.2. Nanomaterial selection and preparation

The nanomaterials in this study—AuNPs, AgNPs and SWCNTs—were chosen for the reason that they have attracted substantial research efforts for potential biomedical and energy applications (Banerjee *et al* 2010, Liu *et al* 2010, Alwarappan and Li 2010, Alwarappan *et al* 2009, Li *et al* 2008).

2.2.1. Synthesis of AuNPs. Hydrogen tetrachloroaurate ($HAuCL_4$) (40 ml, 1.0 mM) was added to an Erlenmeyer flask (250 ml), stirred and brought to the boil on a hotplate. Trisodium citrate ($Na_3C_6H_5O_7$) (4 ml, 1%) was added to the boiling solution. Three minutes after the addition of trisodium citrate, 100 nm Au particles were formed and if the solution was stirred for further 10 min 10 nm AuNPs were formed. Phase imaging and force spectroscopy were performed by AFM and TEM to characterize the nanoparticles.

2.2.2. Synthesis of AgNPs. Sodium borohydride ($NaBH_4$) (60 ml, 2 mM) was added to an Erlenmeyer flask (250 ml) placed in an ice-bath and stirred. To this, silver nitrate ($AgNO_3$) (4 ml, 1.0 mM) solution was added and stirred. Three minutes after the addition of silver nitrate, 100 nm Ag particles were formed and upon stirring for 30 more minutes, 10 nm Ag particles were formed. Phase imaging and force spectroscopy were performed by AFM and TEM to characterize the nanoparticles.

2.2.3. Preparation of SWCNTs. The SWCNTs were placed into a 3:1 mixture of 95% H_2SO_4–60% HNO_3. The solution was sonicated for 5 h and following this the sample was dried in an oven for 24 h. Phase imaging and force spectroscopy were performed by AFM and TEM to characterize the nanoparticles.

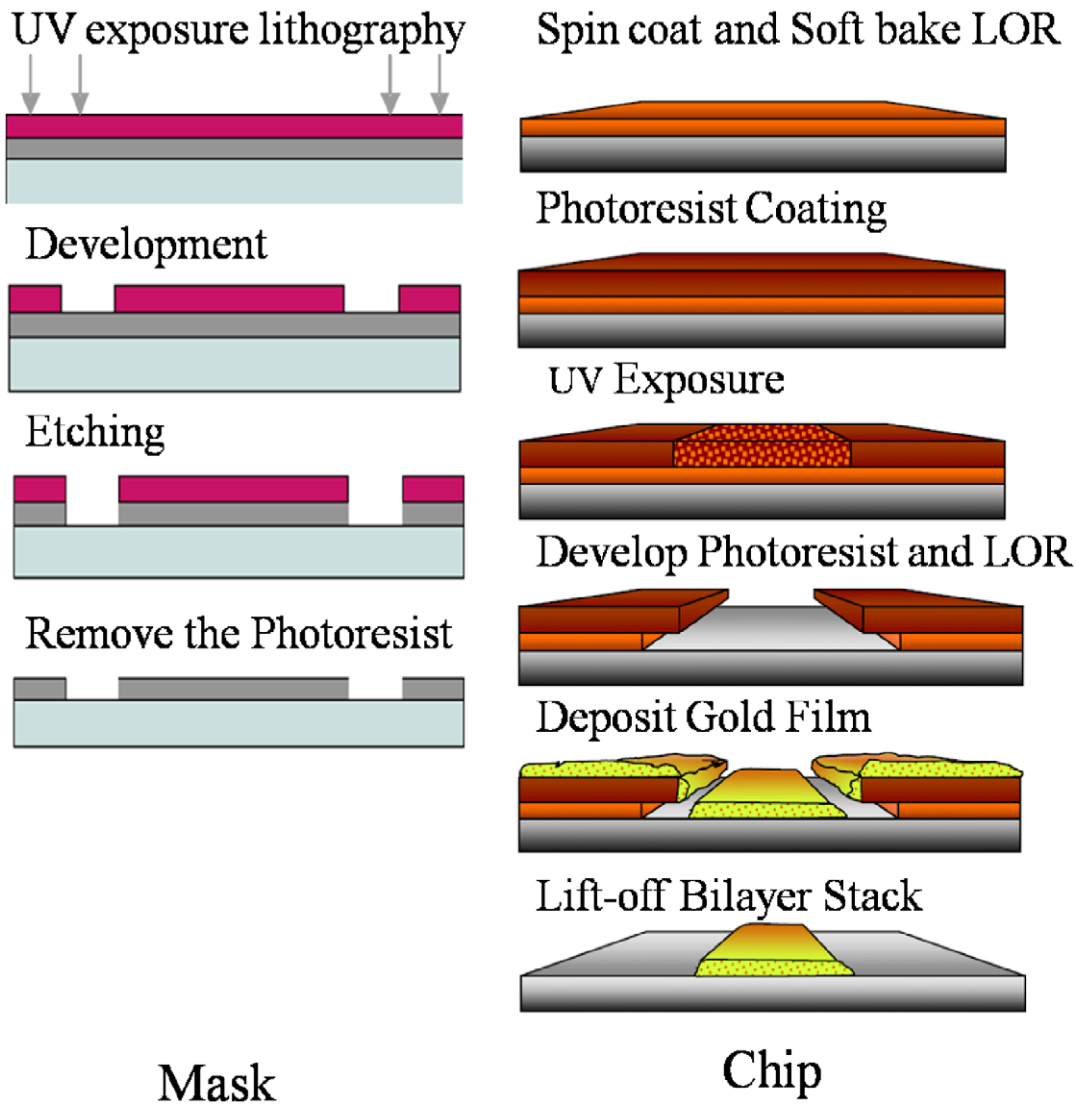

Figure 1. Flow diagram of fabrication of the mask (left) and the array chip (right).

2.3. Cell culture

CCL-153™ and RTgill-W1™ cells were purchased from American Type Culture Collection (ATCC, Rockville, MD, USA) and were cultured in F-12K medium and Leibovitz's L-15 medium, respectively, with each of the media containing 10% fetal bovine serum, 0.3 mg ml^{-1} L-glutamine, 100 U ml^{-1} penicillin and 100 mg ml^{-1} streptomycin. The cell cultures were placed in an incubator (37 °C, 5% CO_2 atmosphere) for 24 h prior to the experiment so that the cells reached confluency with a final concentration of 10^6 cells ml^{-1}. 0.4 ml of cell suspension was inoculated into each well in the EIS chip for the experiment.

2.4. EIS chip fabrication

Photolithographic technology was employed for the gold patterning of the microelectrode array on the substrate. A mask defines the area of the chip that will be exposed to UV light. The mask is placed on top of the photoresist during the exposure process so that only the photoresist under the transparent part of the mask gets exposed. Our fabrication procedure required two lithography masks, one for defining the pattern of the gold electrode circuit and the other for defining the *SU*-8 isolating polymer layer. The masks were made by sputtering a thin chromium layer on a 4′ × 4′ glass slide. A positive photoresist (AZ1518) was spin coated on top of the thin chromium layer. Figure 1 illustrates the flow diagrams of the fabrication of the mask on the left and the microelectrode array on the right.

2.4.1. Substrate cleaning and dehydration. To provide a conductive and transparent sidewall for both electrochemical and optical monitoring, a clear microscope slide was used as the substrate. The slide was cleaned with acetone, rinsed with deionized (DI) water and then baked at 200 °C for 5 min on a contact hotplate.

2.4.2. Sacrifice layer coating. MicroChem's LOR 3B was spin coated at 2500 rpm for 45 s followed by 10 min of baking

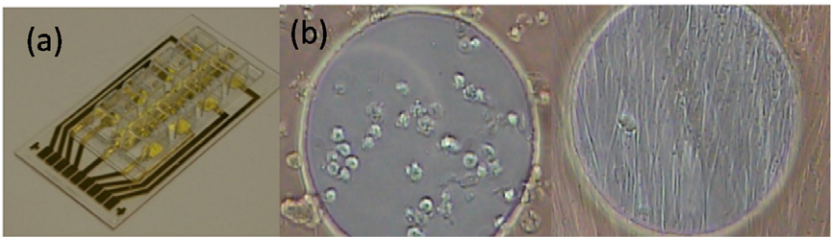

Figure 2. (a) Design of the EIS chip showing the array of eight detecting gold electrodes. (b) Cells on the electrode, before (left) and after (right) attachment.

on a hotplate at 150 °C. On top of the LOR layer, AZ1518 positive photoresist was spin coated at 3500 rpm for 45 s and baked in the oven at 110 °C for 6 min.

2.4.3. Exposure and development. After baking, the photoresist was exposed through a mask under 12.5 mW cm^{-2} for 15 s (total dose is 187.5 mW cm^{-2}). The slide was then submerged in a 1:4 diluted AZ400K developer for 60 s for development.

2.4.4. Deposition. Ten nanometers of Ti thin film was deposited with a growth rate of 3 nm min^{-1} at room temperature by a rf-magnetron sputtering system (AJA) using a Ti target. After Ti deposition, a 150 nm (7 min) Au thin film was deposited on top of the Ti thin film. Both the Ti and Au deposition was done in Ar ambient (10 sccm flow rate) at 75 W of rf power, 5 mTorr pressure and room temperature.

2.4.5. Lift-off. The slide was then submerged in MicroChem's Remover PG and the sacrificial layer was dissolved to form the desired pattern.

2.4.6. Protection layer coating. *SU*-8 was spin coated onto the slide at 2000 rpm for 45 s followed by 13 min of baking on a hotplate at 95 °C.

2.4.7. Final exposure and development The photoresist was exposed through the mask under 12.5 mW cm^{-2} for 24 s (total dose is 300 mW cm^{-2}) and then baked on a hotplate for 16 min at 95 °C. The substrate was finally dipped in *SU*-8 developer for 4 min, and rinsed with IPA and DI water.

2.5. Electrochemical measurements

Cyclic voltammetric and differential pulse voltammetric measurements were carried out using a CHI-630A electrochemical analyzer (CH Instruments, Inc., Austin, TX, USA). The required redox solutions were freshly prepared every day before the start of experiments. PBS (0.1 M) containing Na_2HPO_4 (50 mM), KH_2PO_4 (50 mM) and KCl (100 mM) was adjusted to pH 7.2 by adding NaOH (0.1 M).

2.6. AFM and TEM

Phase imaging and force spectroscopy were performed by using a Multimode Nanoscope IIIa system from Veeco Instruments (Santa Barbara, CA, USA) in air with a relative humidity 40–50% at room temperature.

A 200 keV transmission electron microscope (Hitachi HF-2000 FEG) was used to analyze the structure and composition of the nanomaterials. The TEM samples were dispersed in ethanol followed by sonication for 15 min. The suspension was placed onto a copper grid covered with a carbon thin film for analysis.

2.7. Sulforhodamine B (SRB) assay

The sulforhodamine B (SRB) assay was used for comparison of results by measuring cell density based on the measurement of cellular protein content. SRB is commonly used for toxicity screening of materials to adherent cells. CCL-153™ and RTgill-W1™ were inoculated in a 12-well plate with a concentration of 10^6 cells ml^{-1} in each well. After an incubation period of 48 h, the cell monolayers were fixed with 10% (wt/vol) trichloroacetic acid and stained for 30 min, after which the excess dye was removed by washing repeatedly with 1% (vol/vol) acetic acid. The protein-bound dye was dissolved in 10 mM Tris base solution for optical density determination at 510 nm using a microplate reader.

3. Results and discussion

3.1. Impedance and resistance measurements using EIS chip

The EIS chip design (figure 2(a)) consists of an array of eight detecting gold electrodes (250 μm in diameter) each on the bottom of individual tissue culture wells of volume $9 \times 9 \times 10$ mm^3 to measure the change in impedance to AC current flow (approximately 1 μA). A gold counter electrode (7×46 mm^2) is linked to each individual detecting electrode. To provide a conductive and transparent sidewall for both electrochemical and optical monitoring, a clear microscope slide ($3'' \times 1.5'' \times 1.2$ mm) was used as the substrate, on top of which a 200 nm thick gold thin film was patterned by photolithographic technology based upon the designed electrical circuit. Since the sensing mechanism of the system is based upon the measurement of electrode surface resistances, the electrode surface area plays an important role in the sensitivities. The impedance of the circuit with a resistance (R) and a capacitor (C) in series can be measured for each well by applying an alternating potential (AC) to the two electrodes present in the EIS chip through a 1 MΩ resistor. Cells are placed in each well, drift downward and attach themselves onto the electrode surface over time (figure 2(b)). The current flowing though each electrode is now impeded by

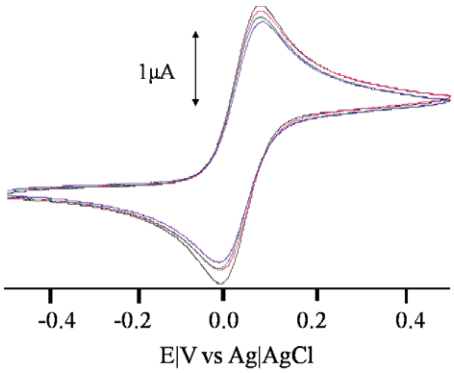

Figure 3. Cyclic voltammogram of four electrodes on the fabricated EIS chip demonstrating the reproducibility of electrochemical activities of the fabricated gold microelectrodes.

the cell monolayer, increasing the impedance and resistance measurements. The smaller sized detecting electrode will dominate the overall impedance in the circuit which will increase in just a few hours as the cells gradually attach to the surface. From Ohm's law, $V = IR$, it is possible to monitor the cell attachment and proliferation from the increase in impedance or resistance measurements.

Using this system, nanotoxicity measurements can be made by monitoring the change in resistance of each electrode. An extremely toxic material would cause the cells to die and detach from the electrode at a rapid rate which, in turn, would decrease the resistance reading of the system. On the other hand, a nontoxic material would not affect the attachment of the cells; hence the resistance measurements would be similar to the measurements of the cells by themselves (control).

An array design was chosen for the electrodes because of its potential to measure multiple experimental designs simultaneously, allowing side by side comparison of the various nanomaterials tested. This design also allows for relatively short measurement times as the EIS is able to detect any interference in cell attachment within a few hours.

3.2. Electrochemical characterization of the EIS chip

Quality electrochemical testing of the chips immediately before the measurements will markedly increase the reliability of the chip's performance. *In situ* chip testing not only provides the possibility to correct minor chip fabrication errors, but also allows rejection of chips which might have been damaged due to improper storage or handling (e.g. at excessive temperatures). The electrochemical testing was carried out by running cyclic voltammetry (CV) using a potassium ferricyanide ($Fe(CN)_6^{3-/4-}$) redox probe. CV is the most widely used technique for acquiring qualitative information about electrochemical reactions. During the potential sweep, the potentiostat measures the redox current resulting from the applied potential using the Randles–Sevcik equation (Bard and Faulkner 2001):

$$i_p = (2.69 \times 10^5) n^{3/2} A C D^{1/2} v^{1/2} \quad (1)$$

where i_p is the peak current, n is the number of electrons, F is the Faraday constant, T is the temperature in kelvin, R is the gas constant, A is the surface area of the working electrode, D is the diffusion coefficient of the electroactive species, C is the bulk concentration of the electroactive species and v is the scan rate of voltammograms.

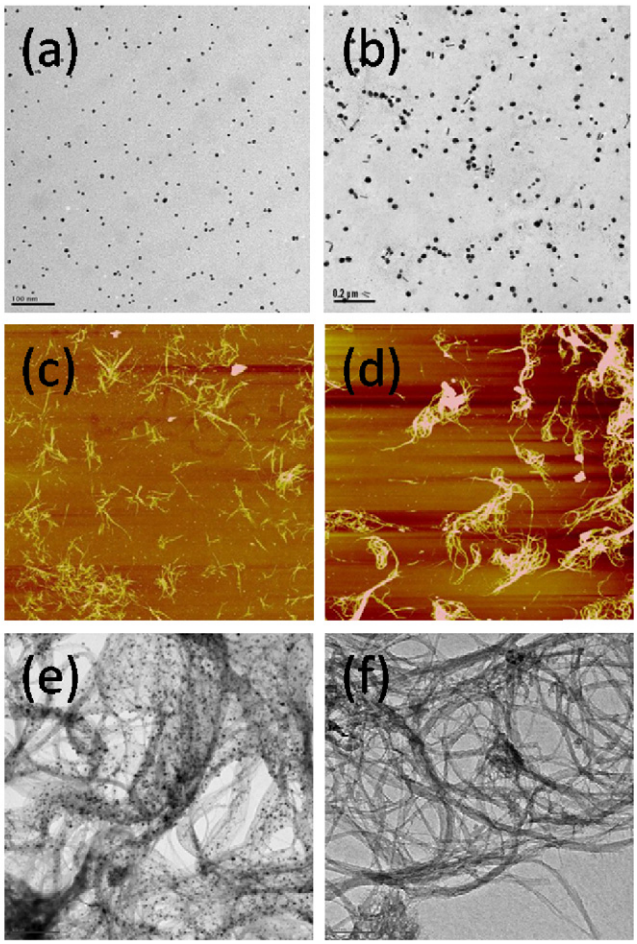

Figure 4. Transmission electron microscopy imaging of: (a) AuNPs (10 nm), (b) AgNPs (10 nm), (c) cut SWCNTs, (d) SWCNTs, (e) raw SWCNTs and (f) purified SWCNTs.

The sensing electrode activity and the actual active electrode surface can be best understood by carefully examining the current–concentration profiles during the potential sweep. Four observables from the cyclic voltammetric response, the two peak currents and two peak potentials, provide the basis for quality testing of the sensing electrodes.

The functionality of the EIS chip was measured by performing cyclic voltammetry in $Fe(CN)_6^{3-/4-}$ (figure 3). The gold microelectrodes designed in our laboratory exhibited reversibility ($\Delta E_p = 64$ mV) with a 6% attenuation in the observed peak current value after four consecutive cycles showing high electrochemical activity and reproducible responses of the redox probes.

3.3. Nanomaterial characterization

The nanoparticles tested in this study, AuNPs (10, 100 nm), AgNPs (10, 100 nm) and SWCNTs (cut, uncut), were all characterized using TEM and AFM (figure 4). Nanomaterial

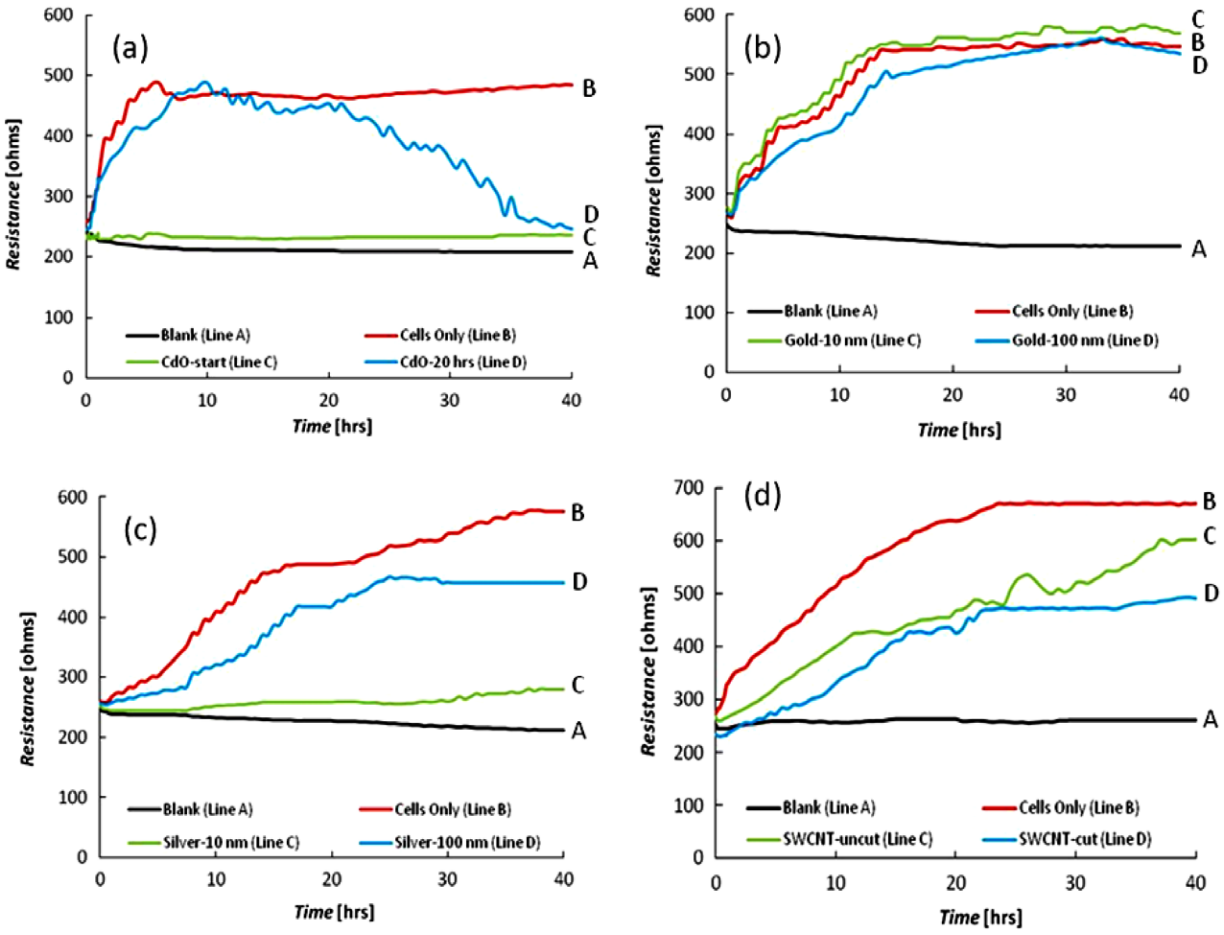

Figure 5. Resistance readings for CdO (a), Au (b), Ag (c) and SWCNT (d) on CCL-153. Lines A and B in all graphs represent the Blank and the Control (cells only) resistance readings. In (a), CdO is added initially (line C) and after 20 hours of cell attachment (line D). In (b), lines C and D represent AuNPS sized 10 nm and 100 nm respectively. In (c), lines C and D represent AgNPS sized 10 nm and 100 nm respectively, and in (d), lines C and D represent the cut and uncut SWCNTs respectively.

characterization is necessary as specific properties of the materials depend on their size and purity. The SWCNTs used in this study were purified in diluted acids. Purified SWCNTs were tested to prevent unwanted contamination of impurities such as amorphous carbon, graphite and catalyst metal particles which may reside on the tubes.

The AuNPs and AgNPs were fabricated at different sizes (10 and 100 nm) to further understand the size effects of the particles and the underlying mechanisms that govern the uptake of nanoparticles into cells. Most cell types undergo phagocytosis or endocytosis to eliminate large particles that interact with the cell membrane; however, the smaller sized particles may bypass the natural mechanical barriers of the cells which may result in severe tissue damage (Barnes *et al* 2003). Once inside the cells, the nanoparticles may interfere with the functions of the cell's organelles and other biomolecular structures leading to damage and even death of the cell. The exact mechanisms of this process are still not fully understood (Brayner 2008, Connor *et al* 2005). However, with the EIS, the affects of the cellular uptake of the nanoparticles on the proliferation of the cells will be demonstrated.

3.4. Cell exposure to cadmium oxide

CdO, which is extremely toxic, was employed to demonstrate the ability of the EIS to measure kinetic effects of the nanoparticles before and after exposure to both CCL-153 and RTgill-W1 cell lines. Cadmium is a toxic material that has been shown to cause lysosomal damage and DNA breakage in mammalian cells and disrupt mitochondrial function and promote apoptosis (Tian *et al* 2006).

In the first setup, the CdO was added to the wells along with the cells in the beginning of the experimental run. This was done to observe the rapid toxic effects of the CdO towards the cells. The resistance changes produced by the attachment of cells to the electrodes were monitored over a 40 h time period (figures 5(a) and 6(a) green lines (C lines)). Results indicated that upon inoculation of the CdO particles, a steady resistance value was observed (similar to the resistance value of the blank) indicating disruption in cell attachment. In the second setup, the cells were allowed to grow on the electrode to confluency over a period of 20 h before the CdO was added. This setup would provide the kinetics of the interaction of CdO with the cells. Once the CdO was added to the cells, we

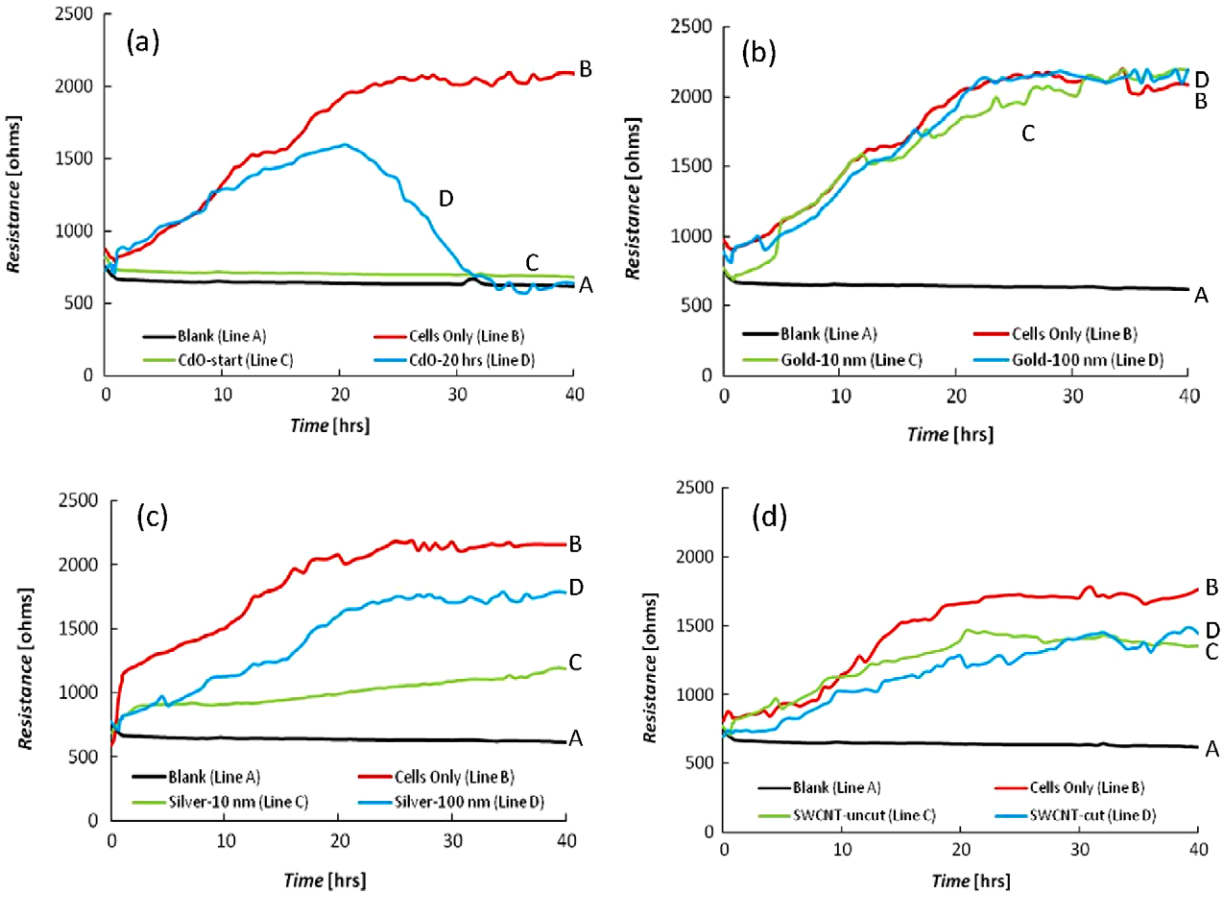

Figure 6. Resistance readings for CdO (a), Au (b), Ag (c) and SWCNT (d) on RTgill-W1. Lines A and B in all graphs represent the Blank and the Control (cells only) resistance readings. In (a), CdO is added initially (line C) and after 20 hours of cell attachment (line D). In (b), lines C and D represent AuNPS sized 10 nm and 100 nm respectively. In (c), lines C and D represent AgNPS sized 10 nm and 100 nm respectively, and in (d), lines C and D represent the cut and uncut SWCNTs respectively.

observed a rapid decrease in the resistance values measured, eventually returning to readings similar to the blank, indicating cell detachment and the harsh cytotoxic effect of CdO towards both CCL-153 and RTgill-W1 (figures 5(a) and 6(a) blue lines (D lines)). These results demonstrate the capability of the EIS to monitor cytotoxicity instantaneously and continuously.

3.5. Cell exposure to gold and silver nanoparticles

AuNPs have been reported to exhibit inert properties, as previous studies have shown that AuNPs with a size less than 100 nm did not induce any adverse effects in human cells (Brayner 2008, Connor *et al* 2005). Due to these inert properties, AuNPs are often employed in research for various applications such as gene and drug delivery transfection vectors, DNA-binding agents and in various imaging systems (Ghosh *et al* 2008).

The cytotoxic measurements of AuNPs (10, 100 nm) towards CCL-153 and RTgill-W1 over a 40 h time period showed little difference in resistance values to those observed for the control (figures 5(b) and 6(b) green and blue lines (C and D lines) respectively). From this observation, it is evident that AuNPs have few cytotoxic effects on both the CCL-153 and the RTgill-W1.

In contrast, Ag has been shown to exhibit a strong toxicity to a wide range of micro-organisms and is widely used in antibacterial solutions (Elechiguerra *et al* 2005), and when eukaryotic cells are exposed to Ag nanoparticles an apoptotic effect is noticed (Arora *et al* 2009). When CCL-153 and RTgill-W1 cells were both exposed to AgNPs (10, 100 nm) noticeable changes in resistance were observed. The measurements for the 100 nm AgNPs exhibited overall lower resistance values compared to the control, indicating a slower attachment rate of the cells (figures 5(c) and 6(c) green lines (C lines)). However, for the 10 nm sized particles, the resistance changes were very small, almost negligible, showing a stronger cytotoxicity for the smaller particles (figures 5(c) and 6(c) blue lines (D lines)). The observed phenomena may be attributed to the fact that the smaller AgNPs can enter the cell easily and possibly interfere with the cellular mechanism thereby decreasing the cell attachment and thus lowering the resistance values.

3.6. Cell exposure to SWCNTs

Rapid advancements in SWCNTs research call for a clearer picture of their cytotoxicity as the effects of SWCNT surface chemistry, surface area and aggregation on the cell cycle is not well established (Tian *et al* 2006). Further, the length of the

Table 1. Optical density values obtained from the SRB assay on CCL-153.

Column1	Optical density
Control	2.7
CdO	0.6
AuNPs (10 nm)	2.5
AuNPs (100 nm)	2.6
AgNPs (10 nm)	1.3
AuNPs (100 nm)	1.6
SWCNTs (cut)	2.2
SWCNTs (uncut)	2.1

SWCNTs is an important factor to consider, as it is evident from previous works that ultra-short SWCNTs can be used as reinforcing agents to enhance the mechanical properties of certain polymers in various biomedical applications (Xinfeng *et al* 2008). Shorter SWCNTs may affect the cells in a different manner than their longer counterparts as they may enter and damage the cells more easily.

We have thus evaluated the cytotoxic effect of SWCNTs (cut and uncut) on CCL-153 and RTgill-W1 cells by monitoring the resistance values over 40 h. Results indicated that the SWCNTs (cut and uncut) exhibited a similar decrease in the resistance value to the control (figures 5(d) and 6(d) green and blue lines (C and D lines) respectively). From this, it is evident that SWCNTs affected the growth mechanism of the CCL-153 and RTgill-W1.

3.7. Sulforhodamine B (SRB) assay

The optical density values obtained from the SRB assay correlate with total protein content and therefore with cell number. Table 1 lists the values obtained for the SRB assays with CdO, AuNPs, AgNPs and SWCNTs.

4. Conclusions

With the increasing number of nanomaterial applications, assessing their toxicity should be the first important step toward creating safety guidelines for their handling and disposal. In this work, we have successfully designed an EIS chip and evaluated its suitability for various cytotoxicity measurements by electrochemical experiments. Results indicated that the EIS chip exhibited a stable and reproducible response when measuring the affects of various nanomaterials—AuNPs (10, 100 nm), AgNPs (10, 100 nm), SWCNTs (cut, uncut) and CdO—towards CCL-153 and RTgill-W1 cells. Moreover, the EIS chip was sensitive enough to measure the micro-motion of a cell and therefore was able to monitor the progression of the cytotoxicity demonstrating the kinetic effects of the nanoparticles on the cells. Further, the EIS chip allowed rapid, real-time and multi-sample analysis creating a versatile, noninvasive tool that is able to provide quantitative information with respect to alteration in cellular function under various nanomaterial exposures.

Acknowledgments

This research work is partially supported under grant FA9550-06-1-046 and FA9550-07-1-0344 of Department of Defense/Air Force Office of Scientific Research, Wallace H Coulter Young Inventor Award, NSF MRI 0821582 and 2008 FIU Faculty Research Award. We would like to thank the Advanced Material Engineering Research Institute (AMERI) at FIU for allowing us to use the MEMS facilities.

References

Alwarappan S and Li C-Z 2010 Simultaneous detection of dopamine, ascorbic acid and uric acid at electrochemically activated carbon nanotube biosensors *Nanomed. Nanotechnol. Biol. Med.* **6** 52–7

Alwarappan S, Prabhulkar S, Durygin A and Li C-Z 2009 The effect of electrochemical pretreatment on the sensing performance of single walled carbon nanotubes *J. Nanosci. Nanotechnol.* **9** 2991–6

Arora S, Jain J, Rajwade J M and Paknikar K M 2009 Interactions of silver nanoparticles with primary mouse fibroblasts and liver cells *Toxicol. Appl. Pharmacol.* **236** 310–8

Banerjee R, Katsenovich Y, Lagos L, Senn M, Naja M, Balsamo V, Pannell K H and Li C-Z 2010 Functional magnetic nanoshells integrated nanosensor for trace analysis of environmental uranium contamination *Electrochim. Acta.* doi:10.1016/j.electacta.2010.05.060

Bard A J and Faulkner L R 2001 *Electrochemical Methods: Fundamental and Applications* 2nd edn (New York: Wiley)

Barnes P J, Shapiro S D and Pauwels R A 2003 Chronic obstructive pulmonary disease: molecular and cellular mechanisms *Eur. Respir. J.* **22** 672–88

Brayner R 2008 The toxicological impact of nanoparticles *Nano Today* **3** 48–55

Connor E E, Mwamuka J, Gole A, Murphy C J and Wyatt M D 2005 Gold nanoparticles are taken up by human cells but do not cause acute cytotoxicity *Small* **1** 325–7

Elder A, Vidyasagar S and DeLouise L 2009 Physicochemical factors that affect metal and metal oxide nanoparticle passage across epithelial barriers *WIREs Nanomed. Nanobiotechnol.* **1** 434–50

Elechiguerra J L, Burt J L, Morones J R, Camacho-Bragado A, Gao X, Lara H H and Yacaman M J 2005 Interaction of silver nanoparticles with HIV-1 *J. Nanobiotechnol.* **3** 6

Ghosh P S, Kim C K, Han G, Forbes N S and Rotello V M 2008 Efficient gene delivery vectors by tuning the surface charge density of amino acid-functionalized gold nanoparticles *ACS Nano* **2** 2213–8

Hussain S M, Hess K L, Gearhart J M, Geiss K T and Schlager J J 2005 *In vitro* toxicity of nanoparticles in BRL 3A rat liver cells *Toxicol. In Vitro* **19** 975–83

Kreyling W G, Semmler-Behnke M and Moller W 2006 Health implications of nanoparticles *J. Nanopart. Res.* **8** 543–62

Lewinski N, Colvin V and Drezek R 2008 Cytotoxicity of nanoparticles *Small* **4** 26–49

Li C-Z, Choi W-B and Chuang C-H 2008 Enhancement of photocurrents by finite-sized SWNT based thin films *Electrochim. Acta* **54** 821–8

Liu C, Alwarappan S and Li C-Z 2010 Design and Characterization of novel membraneless enzymatic biofuel cell based on graphene nanosheets *Biosens. Bioelectron.* **7** 1829–33

Luong J H T, Male K B and Glennon J D 2008 Biosensor technology: technology push versus market pull *Biotechnol. Adv.* **26** 492–500

Mossman B T, Borm P J, Castranova V, Costa D L, Donaldson K and Kleeberger S R 2007 Mechanisms of action of inhaled fibers, particles and nanoparticles in lung and cardiovascular diseases *Part. Fibre Toxicol.* **4** 1–4

Oberdörster G *et al* 2005 Principles for characterizing the potential human health effects from exposure to nanomaterials: elements of a screening strategy *Environ. Health Perspect.* **113** 823–39

Soto K F, Carrasco A, Powell T G, Garza K M and Murr L E 2005 Comparative *in vitro* cytotoxicity assessment of some manufactured nanoparticulate materials characterized by transmission electron microscopy *J. Nanopart. Res.* **7** 145–69

Tian F, Cui D, Schwarz H, Estrada G G and Kobayashi H 2006 Cytotoxicity of single-wall carbon nanotubes on human fibroblasts *Toxicol. In Vitro* **20** 1202–12

Wilhelm C, Gazeau F, Roger J, Pons J N and Bacri J C 2002 Interaction of anionic superparamagnetic nanoparticles with cells: kinetic analyses of membrane adsorption and subsequent internalization *Langmuir* **18** 8148–55

Xinfeng S, Balaji S, Quynh P P, Patrick P S, Jared L H, Lon J W, James M T, Robert M R and Antonios G M 2008 *In vitro* cytotoxicity of single-walled carbon nanotube/biodegradable polymer nanocomposites *J. Biomed. Mater. Res.* A **86** 813–23